Dynamical Behavior of the Dissipative Two-State System

Klaus Völker
Department of Physics and Astronomy, University of California, Los Angeles, CA 90095
(February 1, 2008)

We investigate the dynamical correlation function of a quantum-mechanical two-state system which is coupled to a bosonic heat bath, utilizing the equivalence between the spin-boson Hamiltonian and the $1/r^2$ Ising model. The imaginary-time correlation function is obtained from Monte Carlo simulations on the Ising system and then continued to real time by a Padé approximation. In the unbiased system, the transition from oscillatory to strongly damped behavior is found to occur at a coupling strength close to $\alpha = 1/2$. The biased system favors coherent relaxation and displays a significantly larger crossover value α_c. We introduce the quasiparticle picture to describe the relevant behavior at intermediate time scales. Within this approximation, we map out phase diagrams for the unbiased and biased systems.

Phys. Rev. B **58**, 1862 (1998); PACS numbers: 72.15.Qm 71.27.+a 75.20.Hr

I. INTRODUCTION

The quantum mechanical two-state system, coupled to a dissipative environment, provides a universal model for many physical systems. An important example of current interest is the problem of defect-tunneling in solids.[1] Our interest in this problem was renewed when connections between current topics in high temperature superconductivity[2] and quantum Hall effect[3] were perceived. In fact, all systems that can be described by a double-well potential associated with a generalized coordinate, with appropriate restrictions on the parameters, reduce to a two-state system at sufficiently low temperatures, when only the ground states of the two individual wells remain relevant.[4]

At low temperatures, we can choose the localized ground states of the two potential wells, in the absence of tunneling, as the basis of our two-dimensional Hilbert space. The overlap of the two wavefunctions leads to quantum mechanical tunneling, described by a transition matrix element between the two effective states of the system. Decoupled from its environment, we can write the Hamiltonian of the system in pseudospin language as

$$H_0 = -\frac{\Delta}{2}\sigma_x + \frac{\epsilon}{2}\sigma_z. \tag{1}$$

σ_x and σ_z are the usual Pauli matrices, so that $\Delta/2$ is the tunneling matrix element, and ϵ describes the bias of the system, i.e., the difference in the ground state energies of the two localized states. The isolated system is trivial to diagonalize and exhibits coherent tunneling between the two states.

If the system is coupled to a dissipative environment[5], we can expect the tunneling to lose its phase coherence. This can happen even at zero temperature if the continuous spectrum of the macroscopic dissipative environment extends down to zero frequency. A particularly elegant model of the environment has been known for some time.[4] In this model, a set of harmonic oscillators are coupled linearly to σ_z. The full Hamiltonian is

$$H = -\frac{\Delta}{2}\sigma_x + \frac{\epsilon}{2}\sigma_z + \sum_\alpha \omega_\alpha a_\alpha^\dagger a_\alpha + \frac{\sigma_z}{2}\sum_\alpha f_\alpha (a_\alpha^\dagger + a_\alpha), \tag{2}$$

where the a_α are destruction operators of the harmonic oscillators with frequencies ω_α. The quantity f_α represents the coupling strength of the two-state system to the coordinate of the α^{th} oscillator. This is also known as the spin-boson Hamiltonian[4] that was proposed in the context of a model of a local magnetic impurity coupled by spin-flip scattering to the conduction electrons of the host metal, known as the Kondo problem. The low-energy particle-hole excitations of the conduction electrons define the oscillator states. The environment is completely characterized by its spectral density $J(\omega)$

$$J(\omega) = \frac{\pi}{2}\sum_\alpha f_\alpha^2\,\delta(\omega - \omega_\alpha), \tag{3}$$

As a model of a linear dissipative environment, we consider an Ohmic environment that classically exhibits friction of the form $F = -\eta\dot{q}$, and is described by the spectral density[4]:

$$J(\omega) = \begin{cases} 2\pi\alpha\omega, & \omega \ll \omega_c \\ 0, & \omega \gg \omega_c \end{cases}. \tag{4}$$

The assumption of an Ohmic bath reduces the characteristics of the environment to two parameters, the dimensionless coupling strength α and the characteristic cutoff scale ω_c. The generality of this model is not obvious, unless the phenomena to be studied are strongly dominated by low energy processes. Indeed, the results of the present paper can be trusted for only such low energy processes, which are akin to dynamic quantum critical phenomena. We shall be interested in the dynamical correlation function

$$C(t) = \frac{1}{2i} \langle [\sigma_z(t), \sigma_z(0)] \rangle \,, \tag{5}$$

or its Fourier transform, the response function $\chi''(\omega)$, at zero temperature. In particular, we will consider its qualitative and quantitative dependencies on the parameters Δ, ϵ and α, appearing in the guise of dimensionless ratios Δ/ω_c and ϵ/ω_c ($\hbar$ and k_B are set to unity).

In an analogous model, one can also couple a two-state system to a Fermionic environment that can be described by a non-interacting set of quasiparticles,[6] or to a Fermi liquid. Except for certain restrictions on parameters, this is equivalent to the oscillator model for the low-energy states of the tunneling degree of freedom. More intriguing, however, is the case where the tunneling degree of freedom is coupled to a Luttinger liquid as in a quasi-one-dimensional electron gas, or to the edge states in a quantum Hall system,[3] but this topic is outside the scope of the present paper.

It is known for some time[7] that the partition function of this system can be transformed into the partition function of an Ising model with long-range interactions. A particular Ising site corresponds to the pseudospin state at a particular point on the imaginary-time axis. This connection enables us to determine the imaginary-time correlation function of the two-state system from Monte Carlo simulations of the Ising model. A Wick rotation then leads us from imaginary time to the above mentioned real-time correlation function $C(t)$. This procedure will be described in detail in the following sections and constitutes a reliable *nonperturbative* evaluation of the dynamics of the system in regimes in which dilute blip approximation employed previously is not reliable. The present paper is based on ideas introduced in a short communication by Chakravarty and Rudnick.[8]

We know that the correlation function $C(t)$ will exhibit coherent oscillations for zero coupling. Weak coupling to the environment leads to damped oscillatory behavior. For small α and Δ/ω_c, scaling arguments[9] yield the renormalized tunneling frequency

$$\Delta_r = \Delta \left(\Delta/\omega_c\right)^{\alpha/1-\alpha} . \tag{6}$$

If the influence of the environment is strong enough, we expect a completely incoherent decay of the time correlation function; further increase of the coupling leads to broken symmetry and the tunneling degree of freedom is localized.[10] One aim of the present paper is to map out the coherent and incoherent regimes in a phase diagram, at zero temperature, and to provide quantitative results for the behavior near the crossover value of α. We will also obtain a qualitative picture of the behavior of $C(t)$ in a biased system ($\epsilon \neq 0$).

In Sec. II we will derive the precise correspondence between the spin-boson Hamiltonian and a classical Ising spin system. Section III deals with aspects of the Monte Carlo simulations on the Ising model, and with the Padé approximation method used to obtain real-time results. Those results are presented in Sec. IV. Section V introduces the quasiparticle picture as an elegant way to model the essential physics at intermediate times. Results obtained within the quasiparticle approximation are presented in Secs. VI and VII. The last section compares our results with some exact results for the zero-frequency limit of the spectral function and for the Toulouse case $\alpha = 1/2$.

II. THE DISSIPATIVE TWO-STATE SYSTEM, THE COULOMB GAS MODEL AND THE INVERSE-SQUARE ISING MODEL

The partition function corresponding to the Hamiltonian (2) can be cast into the Coulomb-gas[11] form, that is, a one-dimensional system of alternating positive and negative charges. Expanding the partition function in terms of σ_x in imaginary time, we get:

$$Z = \mathrm{Tr}\Big[e^{-\beta H}\Big] = \mathrm{Tr}\Big[e^{-\beta H_\infty} \sum_{n=0}^{\infty} (-1)^n \times \int_0^\beta d\tau_1 \cdots \int_0^{\tau_{n-1}} d\tau_n \, H_\Delta(\tau_1) \cdots H_\Delta(\tau_n)\Big]. \tag{7}$$

where

$$H_\Delta = -\frac{\Delta}{2}\sigma_x, \tag{8}$$

$$H_\infty = \sum_\alpha \omega_\alpha a_\alpha^\dagger a_\alpha + \frac{\sigma_z}{2}\left(\sum_\alpha f_\alpha (a_\alpha^\dagger + a_\alpha) + \epsilon\right), \tag{9}$$

and $H_\Delta(\tau) = e^{\tau H_\infty} H_\Delta e^{-\tau H_\infty}$ is the operator in the interaction representation. After integrating out the environmental degrees of freedom, we arrive at the following expression for Z:

$$Z = Z_0 \sum_{n=0}^{\infty} \left(\frac{\Delta}{2}\right)^{2n} \int_0^\beta d\tau_1 \cdots \int_0^{\tau_{2n-1}} d\tau_{2n} \times \exp\Big\{-\frac{\epsilon}{2}\int_0^\beta ds\, \xi(s) - \tilde{H}\Big\}, \tag{10}$$

where

$$\tilde{H} = -\frac{1}{8}\sum_\alpha f_\alpha^2 \int_0^\beta ds\, \xi(s) \int_0^\beta ds'\, \xi(s') \times \Big[e^{-\omega_\alpha |s-s'|} + 2n_\alpha \cosh \omega_\alpha (s-s')\Big], \tag{11}$$

$$\xi(s) = \begin{cases} +1, & \tau_{2k} < s < \tau_{2k+1} \\ -1, & \tau_{2k-1} < s < \tau_{2k} \end{cases} = 1 + 2\sum_{n=0}^{\infty} (-1)^n \theta(s - \tau_n), \tag{12}$$

The algebraic manipulations are detailed in Ref. 6. $n_\alpha = 1/(e^{\beta\omega_\alpha}-1)$ is the Bose occupation factor, and Z_0 is the partition function of the environment. At this point we will introduce the explicit form of the spectral density:

$$J(\omega) = \pi \sum_\alpha f_\alpha^2 \delta(\omega-\omega_\alpha) = 2\pi\alpha\omega\tilde{\theta}(\omega/\omega_c). \qquad (13)$$

Here, $\tilde{\theta}(x)$ symbolizes a generic cutoff function: $\tilde{\theta}(x) = 1$ for $x = 0$, $\tilde{\theta}(x) = 0$ for $x \gg 1$, and smooth in between. Then

$$\tilde{H} = -\frac{\alpha}{4}\int_0^\beta ds\,\xi(s)\int_0^\beta ds'\,\xi(s') \times \int_0^\infty dw\, w \frac{\cosh\left[\omega\left(\frac{\beta}{2}-|s-s'|\right)\right]}{\sinh\frac{\beta\omega}{2}}\tilde{\theta}(\omega/\omega_c). \qquad (14)$$

An approximate treatment of the cutoff consists in removing the cutoff from the integral in this expression, and reintroducing it in the form of the regularization condition $|\tau-\tau'| \geq \omega_c^{-1}$ in the partition function (10). This corresponds to a hard-sphere repulsion between the Coulomb gas charges. Then the integral over ω yields:

$$\int_0^\infty dw\, w \frac{\cosh\left[\omega\left(\frac{\beta}{2}-|s-s'|\right)\right]}{\sinh\frac{\beta\omega}{2}} = \left(\frac{\pi}{\beta}\right)^2\left[\sin\left(\frac{\pi}{\beta}|s-s'|\right)\right]^{-2}. \qquad (15)$$

Next we can perform a two-fold partial integration over s and s', noting that the boundary terms are zero and $d\xi/ds = 2\sum_k (-1)^k\delta(s-\tau_k)$, arriving at:

$$Z = Z_0\sum_{n=0}^\infty\left(\frac{\Delta\tau_c}{2}\right)^{2n}\int_0^\beta\frac{d\tau_1}{\tau_c}\int_0^{\tau_1-\tau_c}\frac{d\tau_2}{\tau_c}\cdots \times\int_0^{\tau_{2n-1}-\tau_c}\frac{d\tau_{2n}}{\tau_c}\exp\left\{\epsilon\sum_{j=1}^{2n}(-1)^j\tau_j +2\alpha\sum_{i<j}(-1)^{i+j}\ln\left|\frac{\beta}{\pi\tau_c}\sin\frac{\pi}{\beta}(\tau_j-\tau_i)\right|\right\} \qquad (16)$$

The $\tau_c = 1/\omega_c$ appearing in the upper boundaries of integration is the regularization condition that replaced the high-frequency cutoff in $J(\omega)$. In this picture, the positions τ_j of the charged particles correspond to spin-flips of the two-state system on the imaginary-time axis. It should be emphasized that this treatment of the cutoff is somewhat artificial, and we therefore do not have a complete description of the high-energy details of the system. Note, however, that the logarithm in the above expression (16) vanishes as $\tau-\tau' \to \tau_c$, so that our treatment is self-consistent. A more rigorous treatment would lead to additional terms of the form $(\tau_j-\tau_i)^{-x}, x \geq 1$ in the Hamiltonian. The effects of these terms on the results for intermediate time scales can be summarized by replacing $\Delta\tau_c$ with an effective value $(\Delta\tau_c)_{\rm eff}$. Otherwise, the cutoff procedure does not affect our results for intermediate time scales.[12] Furthermore, since the ln is the only scale invariant term in the series, the additional terms cannot change the critical behavior of the system.[13]

Let us now consider a one-dimensional Ising model with long-range interactions and periodic boundary conditions, given by:

$$Z = \sum_{S_1\cdots S_N}\exp\Big\{-\sum_{j<i}V(i-j)S_iS_j - h\sum_j S_j\Big\}. \qquad (17)$$

Following Cardy,[13] we can rewrite the partition function in terms of interactions between spin flips or kinks:

$$Z = \sum_{n=0}^\infty y^{2n}\int_0^\beta\frac{d\tau_1}{a}\int_0^{\tau_1-a}\frac{d\tau_2}{a}\cdots\int_0^{\tau_{2n-1}-a}\frac{d\tau_{2n}}{a} \times\exp\Big\{\sum_{j<i}(-1)^{i-j}4U\left(\frac{\tau_i-\tau_j}{a}\right) +2h\sum_j(-1)^j\left(\frac{\tau_j}{a}\right)\Big\}, \qquad (18)$$

where $U(k)$ is defined by

$$V(x) = U(k+1) - 2U(k) + U(k-1), \qquad (19)$$

and $y = e^{2U(0)}$ is the chemical potential, or fugacity, of the system.

The short-distance cutoff at $\tau = a$ was introduced to recapture the high-energy properties of the discrete lattice, after allowing the kinks to move in the continuous interval $\tau = 0\cdots Na$. Here, a is the lattice constant of the Ising model. Again, this approximate treatment of the cutoff changes the high-energy behavior of the system, but leaves the low-energy physics invariant, aside from a modification of parameters related to the cutoff.

Comparison with (16) yields $a = \tau_c$ and

$$U(n) = \frac{\alpha}{2}\ln\left|\frac{N}{\pi}\sin\frac{\pi n}{N}\right|, \quad n \geq 1, \qquad (20)$$

so that

$$V(n) = -\frac{\alpha}{2}\frac{(\pi/N)^2}{\sin^2(\pi n/N)}, \quad n \geq 2, \qquad (21)$$

where we neglected terms of order $(\pi/N)^4$. $V(1)$ is determined by $U(0)$, which in turn depends on the fugacity $y = e^{2U(0)} = \Delta\tau_c/2$. In the limit $N \to \infty$ we get:

$$U(0) = V(1) - \frac{\alpha}{2}\gamma, \qquad (22)$$

where $\gamma = 0.577\ldots$ is Euler's constant. In the familiar language of the Ising model, the Hamiltonian reads:

$$\beta_I H_I = -\frac{J_{NN}}{2}\sum_i S_iS_{i+1} - \frac{J_{LR}}{2}\sum_{j<i}\frac{(\pi/N)^2 S_iS_j}{\sin^2[\pi(j-i)/N]} - h\sum_i S_i, \qquad (23)$$

where $J_{LR} = \alpha$, and $J_{NN} + J_{LR} = -2V(1)$, so that $y = e^{-J_{NN}-(1+\gamma)J_{LR}}$. To summarize, the correspondence of the parameters is as follows:

$$\begin{aligned} \frac{\Delta_{eff}}{2\omega_c} &= \exp\{-J_{NN} - (1+\gamma)J_{LR}\}; \\ \alpha &= J_{LR}; \\ \frac{\epsilon}{2\omega_c} &= h; \\ \beta\omega_c &= N. \end{aligned} \tag{24}$$

Finally, the anisotropic spin-half Kondo model can be cast into the same Coulomb gas form.[7] In particular, the case $\alpha = 1/2$ corresponds to the exactly solvable Toulouse limit of the Kondo problem, which constitutes an important check of our numerical results.

III. NUMERICAL TECHNIQUES: MONTE CARLO SIMULATION AND PADÉ APPROXIMATION

Due to the equivalence of both models, a calculation of the spin-spin correlation function $S_I(|i-j|)$ of the Ising model (23) provides us with the imaginary-time correlation function $\mathcal{C}(\tau) = \langle \sigma_z(\tau)\sigma_z(0)\rangle$ of the two-state system. The former can be computed using standard Monte Carlo techniques. Since the regions of parameter space of primary interest to us lie in the vicinity of the Ising model phase transition, the accuracy of standard Monte Carlo algorithms is greatly suppressed by the phenomenon of critical slowing down: The autocorrelation function, which measures the number of Monte Carlo steps necessary to obtain two statistically independent configurations, diverges at the phase boundary. To get a correct picture of the thermodynamics, an extremely high number of lattice sweeps becomes necessary.

To circumvent this problem, we use the Swendsen-Wang algorithm,[14] where the Ising model is mapped onto a percolation model: In every Monte Carlo step, bonds are drawn with probability $P_{ij} = 1 - e^{-J_{ij}}$ between each two parallel spins, and no bonds are drawn ($P_{ij} = 0$) if the spins are antiparallel. The spins do not necessarily have to be nearest neighbors, and J_{ij} is the sum of their nearest-neighbor and long-range interactions. Then, spins which are directly or indirectly connected by bonds are grouped into clusters, and each spin in a cluster is assigned the same spin state with a probability $P_{\uparrow\downarrow} = e^{\pm nh}/(e^{nh} + e^{-nh})$ for spin-up and spin-down, respectively. Here n is the number of spins contained in this particular cluster. It is straightforward to check that the principle of detailed balance is satisfied for this algorithm, so that the distribution of spin states converges to the Boltzmann distribution. Our implementation of the algorithm performs the formation of clusters simultaneously with the assignment of bonds, so that no additional computation time has to be invested here.

Next, the Fourier transform $\mathcal{C}(\omega_n)$ at the Matsubara frequencies is obtained. The Padé approximant method of Vidberg and Serene[15] is used to continue this spectral function from the positive Matsubara frequencies onto the real axis. Essentially, the spectral function is approximated by a rational function, with numerator and denominator polynomials of order $N/2$, where N is the number of Matsubara points used in the approximation. This rational function can then be trivially continued into the complex plane, given that the first quadrant of the plane is free of singularities. The imaginary part of the resulting function is the response function $\chi''(\omega)$, as we shall see below.

The Padé approximation, in the context of analytic continuation, is an ill-defined procedure in the sense that small errors in the input data can lead to severe discrepancies in the output data. Accuracy of the simulation data is therefore a critical issue. We used 8×10^6 Monte Carlo sweeps on a lattice with $N = 256$ Ising spins for most points in parameter space, but had to increase this number in the vicinity of the crossover value of α to 2×10^7 sweeps. The results are essentially independent of $N = \beta\omega_c$, so they converge well in the zero-temperature limit. However, simulations on a finite spin system will not allow us to capture the localization effects[10] that occur for $\alpha \to 1$.

To get a measure for the simulation errors, we calculated the Padé approximant several times for each data point, using different numbers of lattice sweeps and Padé points. The results were filtered by checking the basic analytic structure of $\chi''(\omega)$ and the behavior for $|\omega| \to \infty$.

IV. RESULTS

In this section we present results for the anti-symmetrized correlation function $C(t) = \frac{1}{2i}\langle[\sigma_z(t), \sigma_z(0)]\rangle$ at zero temperature, as obtained from Monte Carlo simulations on the Ising system (23), and continued to real time by a Padé approximation. The analytic continuation is carried out in the complex frequency plane. Therefore we introduce Green's functions corresponding to the correlation functions in imaginary and real time as:

$$\begin{aligned} \mathcal{G}(\tau) &= -\frac{1}{Z}\,\mathrm{Tr}\Big[e^{-\beta H}e^{|\tau|H}\sigma_z e^{-|\tau|H}\sigma_z\Big] = -\mathcal{C}(|\tau|), \\ G(t) &= -\frac{i}{Z}\,\mathrm{Tr}\Big[e^{-\beta H}e^{iH|t|}\sigma_z e^{-iH|t|}\sigma_z\Big] \\ &= -i\,\langle\sigma_z(|t|)\sigma_z(0)\rangle\,. \end{aligned} \tag{25}$$

These Green's functions are bosonic in character ($\mathcal{G}(\tau+\beta) = \mathcal{G}(\tau), \tau < 0$), so that their Fourier transforms are connected in the complex plane as[17]

$$\mathcal{G}(-i\omega_n) = \mathrm{Re}\,G(\omega) + i\,\mathrm{Im}\,G(\omega)\tanh\frac{\beta\omega}{2}, \tag{26}$$

which leads to the following relation between $\mathcal{C}(\tau)$ and the response function $\chi''(\omega)$:

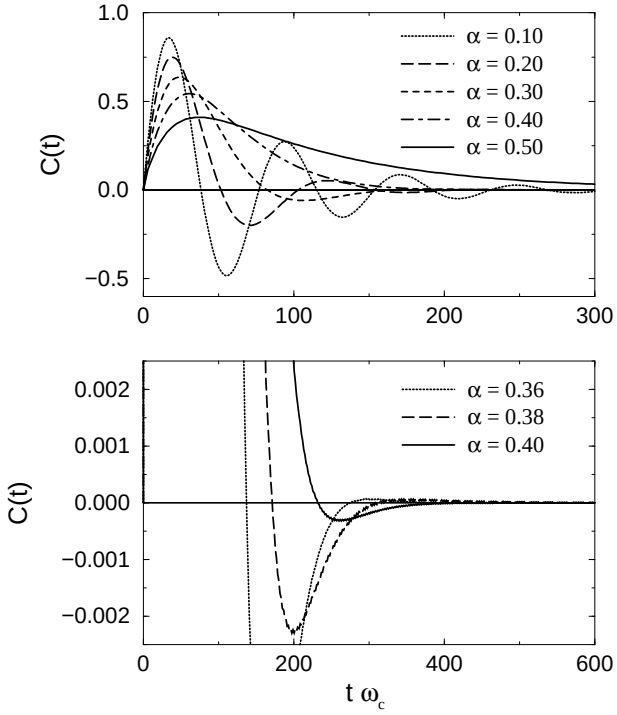

FIG. 1. The correlation function $C(t) = \frac{1}{2i}\langle[\sigma_z(t), \sigma_z(0)]\rangle$ for $\Delta/\omega_c = 0.1$ and different values of α (top). Oscillatory behavior can be observed up to a coupling strength $\alpha = 0.4$ (bottom).

$$\begin{aligned}\chi''(\omega) &= \frac{1}{2}\int_{-\infty}^{\infty} dt\, e^{i\omega t}\langle[\sigma_z(t), \sigma_z(0)]\rangle \\ &= \tanh\left(\frac{\beta\omega}{2}\right)\int_{-\infty}^{\infty} dt\, e^{i\omega t}\mathrm{Re}\langle\sigma_z(t)\sigma_z(0)\rangle \\ &= \mathrm{Im}\,\mathcal{C}(-i\omega). \end{aligned} \tag{27}$$

Figure 1 shows some examples[16] for $C(t)$ in the unbiased case ($\epsilon = 0$), for $\Delta/\omega_c = 0.1$ and various values of α. We can clearly observe coherent, weakly damped oscillations of the form $C(t) = Z\sin(\omega_0 t)\, e^{-\lambda|t|}$ for small values of α. A more detailed plot (Fig. 1 bottom) reveals that oscillations are indeed visible up to $\alpha \simeq 0.4$. Past that value, the accuracy of our numerical data does not allow to resolve oscillatory behavior anymore. Figure 2 shows oscillation frequency ω_0 and damping coefficient λ as obtained from the data in Fig. 1.

In the case of a biased system ($\epsilon \neq 0$, see Fig. 3), the oscillation frequency is greatly enhanced, while the damping coefficient remains largely unaffected by the bias. The oscillations are weaker, since the system dwells in the energetically favored state most of the time.

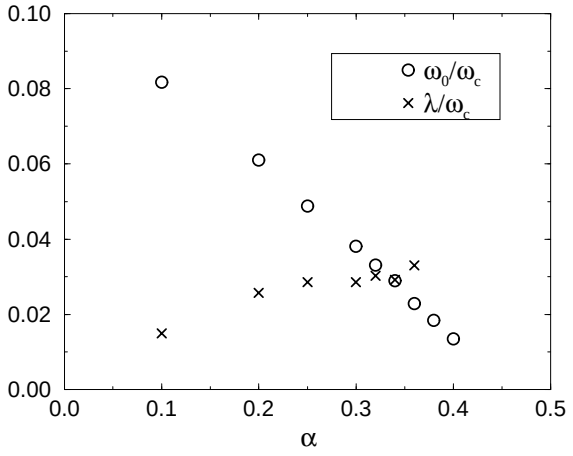

FIG. 2. Oscillation frequency ω_0 and damping coefficient λ corresponding to the curves shown in Fig. 1.

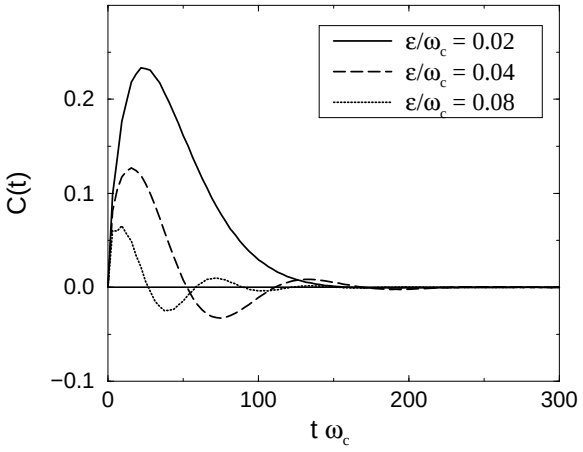

FIG. 3. $C(t)$ for the biased system, for $\Delta/\omega_c = 0.1, \alpha = 0.5$ and various values of ϵ/ω_c. The biased system favors coherent oscillations.

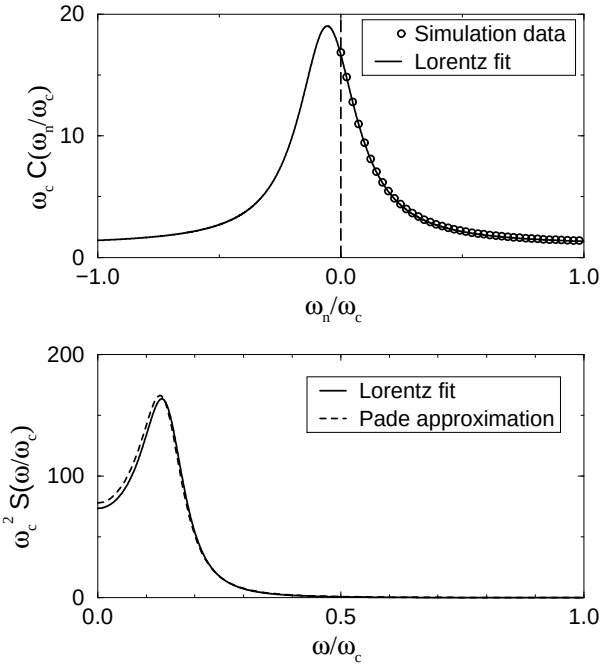

FIG. 4. top: The imaginary-time correlation function $C(\omega_n)$ at the Matsubara frequencies, as obtained from Monte Carlo simulation (circles), for $\Delta/\omega_c = 0.2$, $\alpha = 0.2$, and its approximation by a Lorentzian (solid line). Bottom: Spectral function $S(\omega)$, as calculated from the Lorentz fit (solid line), and by Padé approximation (dashed line).

V. ANALYTIC PROPERTIES OF THE SPECTRAL FUNCTION

An example for the Fourier transform of the imaginary-time correlation function $\mathcal{C}(\omega_n) = \int_0^\beta d\tau\ e^{i\omega_n\tau}\ \mathcal{C}(\tau)$ is shown in Fig. 4. Note that, since $\mathcal{C}(\tau)$ is real and symmetric in τ, only the positive-frequency part has physical meaning. Analytic continuation to negative frequencies reveals, however, that this function is very well described by a Lorentzian:

$$\mathcal{C}(\omega_n) \approx \frac{aw_0^3}{(\omega_n+\lambda)^2+\omega_0^2} + \text{const.} \qquad (28)$$

This approximate form seems to hold extremely well in large parts of parameter space. Typical deviations are of the order of 1%, but become larger close to $\alpha = 1/2$. However, we cannot expect this simple approximation to give reliable results near the crossover value of α, and it will not be used in the following to obtain any quantitative results. In particular, it fails to reproduce the explicit form (38) of the spectral function for the Toulouse case $\alpha = 1/2$.

We consider the spectral function $S(\omega) = \chi''(\omega)/\omega$. According to (27), the approximate form of $S(\omega)$ displays a simple four-pole structure in the complex plane:

$$S(\omega) \equiv \frac{\chi''(\omega)}{\omega} \approx \frac{aQ^{-1}}{[(\omega/\omega_0)^2 - 1 + Q^{-2}]^2 + 4Q^{-2}}. \qquad (29)$$

Here, $Q = \omega_0/\lambda$ is the Q-value of the resonance. ω_0 is the oscillation frequency, and λ the damping coefficient. Again, this simplified form of the spectral function cannot be expected to give reliable quantitative results and will be used solely for illustrative purposes. All results are obtained from Padé approximants to $\mathcal{C}(\omega_n)$ based on up to 256 Matsubara points.

The Quasiparticle Picture

Applying the Padé approximation to obtain the precise form of $S(\omega)$ in the complex plane, we discover that its analytic structure is very similar to that of the Lorentzian approximation (29). It is dominated by four poles at $\omega = \pm\omega_0 \pm i\lambda$, as can be seen in Fig. 5. The physical meaning of these poles requires some consideration: We know from the spectral representation of the correlation function that it has a branch cut along the real axis, and is otherwise free of singularities on the first Riemann sheet. If the spectral density associated with the branch cut is sharply peaked around a finite frequency ω_0, it is legitimate to approximate the dominant part of the spectral density by a simple pole at $\omega_0 + i\lambda$, the "quasiparticle pole", which gives rise to the oscillatory part of the correlation function:

$$C(t) = Z\sin(\omega_0 t)\, e^{-\lambda|t|} + (\text{incoherent part}) \qquad (30)$$

Alternatively, we can view the quasiparticle pole as resulting from an analytic continuation of the spectral function past the branch cut onto the second Riemann sheet. This is done, for example, in Fermi-liquid theory, and accurately reproduces the intermediate-time behavior of the correlation function. The intermediate-time range, over which Fermi-liquid theory is valid, is defined by[18] $1/\epsilon_k \ll t \lesssim 1/\gamma_k$, where ϵ_k and γ_k are quasiparticle energy and damping, respectively. In particular, neither the short-time decay proportional to t nor the exponential long-time decay implied by Fermi-liquid theory reflect the true behavior of the correlation function.

In fact, the Padé approximation naturally yields this analytic continuation past the branch cut, since the existence of a branch cut on the real axis cannot be inferred from the shape of $C(\omega)$ on the imaginary axis. The Padé approximant therefore produces precisely this "quasiparticle picture" of the spectral function. The fact that it does not reveal any other characteristics indicates that almost all of the spectral weight contributes to the quasiparticle peaks. As in Fermi-liquid theory, the quasiparticle picture will reproduce neither the high-energy behavior nor the long-time tail of the correlation function. These are dominated by the incoherent part of the spectral function, which corresponds to other, more complicated singularities in the complex plane.

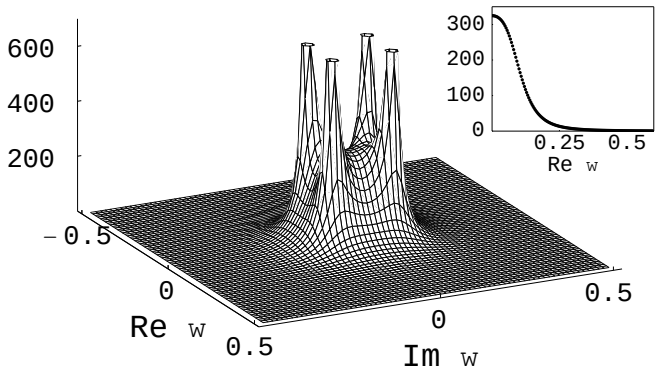

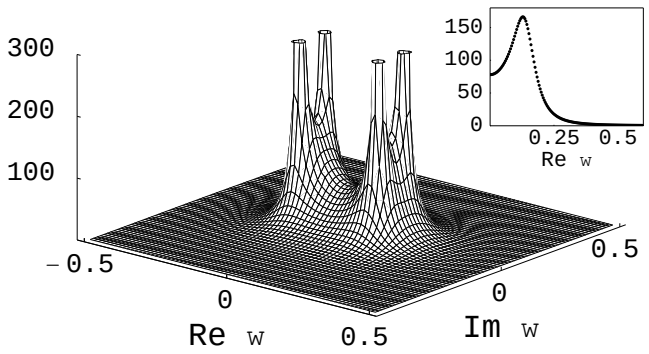

FIG. 5. The absolute value of the spectral function $|S(\omega)|$ in the complex ω plane, as obtained from a Padé approximant using 256 Matsubara points, for $\Delta/\omega_c = 0.2$, and $\alpha = 0.2$ (top), $\alpha = 0.35$ (bottom). The analytic structure is dominated by four poles at $\omega = \pm\omega_0 \pm i\lambda$. The insets show $S(\omega)$ on the positive real axis: the quasiparticle peak is visible only for $\alpha < 0.33$.

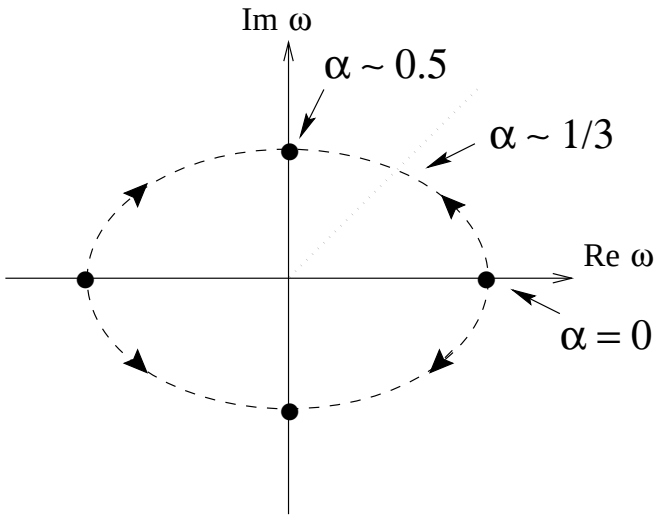

FIG. 6. The journey of the quasiparticle poles in the complex ω-plane

We might also consider the *symmetrized* correlation function

$$C_s(t) = \mathrm{Re}\langle\sigma_z(t)\sigma_z(0)\rangle = \tfrac{1}{2}\,\langle\sigma_z(t)\sigma_z(0) + \sigma_z(0)\sigma_z(t)\rangle\,, \tag{31}$$

which acquires an additional branch cut contribution (at T=0) from the *tanh* factor in Eqn. (27):

$$C_s^{\rm inc}(t) = \int_0^\infty \frac{d\omega}{2\pi}\, e^{-\omega t}\,[\mathcal{C}(\omega) - \mathcal{C}(-\omega)]\,. \tag{32}$$

Here, $\mathcal{C}(-\omega)$ is the analytic continuation of $\mathcal{C}(\omega)$ to negative frequencies. In particular, this term leads to an asymptotic $1/t^2$ decay. When $Q \lesssim 1$, this incoherent background contribution will become dominant at intermediate and short time scales as well, so that in this regime it might be difficult to observe coherent oscillatory behavior experimentally in the symmetrized correlation function $C_s(t)$. As in Fermi-liquid theory, the time interval over which the quasiparticle picture *accurately* describes $C_s(t)$, is bounded by $1/\omega_0 \ll t \lesssim 1/\lambda$, which implies $Q \gg 1$.

Note that these considerations do not apply to the anti-symmetrized correlation function $C(t)$, since the contribution (32) is purely real. For this function, we expect deviations from the quasiparticle behavior only at short-time scales comparable to the inverse cutoff $1/\omega_c$. Furthermore, we have seen in Sec. IV that damped oscillatory behavior is observable at time scales up to a few times the inverse damping coefficient. At longer time scales, a crossover to algebraic decay may also be observed in the anti-symmetrized correlation function $C(t)$.

VI. OSCILLATORY AND DAMPED BEHAVIOR

The results presented here are based on the quasiparticle picture introduced in the previous section. We have

seen in Sec. IV that the quasiparticle picture offers an accurate description of the intermediate-time dynamics at least for coupling strengths up to $\alpha \approx 0.4$. Close to $\alpha = 1/2$, the spectral function may acquire a significant incoherent part due to more complicated singularities in the complex plane, and the quasiparticle picture might not offer an accurate description of the dynamics anymore. Therefore, the results very close to $\alpha = 1/2$ should best be viewed as characteristics of the quasiparticle model.

For $\alpha = 0$ (no coupling to the environment), each two quasiparticle poles coincide on the real axis, yielding the familiar oscillatory behavior of every quantum-mechanical two-state system. As we turn on the coupling ($\alpha > 0$), the poles move away from the real axis into the complex regime, as sketched in Fig. 6, corresponding to weakly damped oscillations. For even larger values of α, the poles meet with the imaginary axis, giving rise to overdamped relaxation.

The location of the poles in the complex plane was obtained numerically from the results of the Padé approximation. Fig. 7 shows the real (ω_0) and imaginary (λ) part of their location as a function of α for different values of Δ/ω_c. Note that the results agree very well with Sec. IV. The real part ω_0 fits nicely to a power-law curve: $\omega_0(\alpha) \sim (\alpha_c - \alpha)^\nu$, $\alpha < \alpha_c$. Since we cannot *ad hoc* assume that the power-law form holds for arbitrary $\alpha < \alpha_c$, only points with $\alpha \geq 0.3$ were included in the fits. With the exception of $\Delta/\omega_c = 0.5$, the graphs follow the power-law form surprisingly well for all $\alpha < \alpha_c$. The results do not change significantly if we limit ourselves to an even smaller number of data points in the vicinity of α_c.

The Q value, $Q = \omega_0/\lambda$, is shown in Fig. 8. The scaling form[9]

$$S(\omega) = \frac{1}{\Delta_r^2} f(\omega/\Delta_r, \alpha), \tag{33}$$

which holds for $\Delta \ll \omega_c$, implies that the Q value is a universal function of α, which is independent of Δ/ω_c. This is indeed the case for $\Delta/\omega_c \lesssim 0.2$ and α not too close to the critical value.

For values of α that are not too large, the oscillatory behavior of the system is visible in the spectral function in the form of inelastic peaks on the real axis, centered around $\omega = \pm\omega_0$. If we increase the damping, the peaks broaden and move closer to the origin. At $Q = 1$, when the half-width of the peaks starts to exceed their separation, they can no longer be distinguished, and the spectral function now appears to be centered at $\omega = 0$, as can easily be verified from the approximate form (29). The Q factor reaches unity when $\alpha \simeq 1/3$, in agreement with results obtained by a numerical renormalization group calculation[19] and an analytic form factor approach[3]. Oscillatory behavior persists beyond that point, however, due to the presence of the quasiparticle poles in the complex plane at nonzero values of ω_0. This was confirmed in Sec. IV without resorting to the quasiparticle picture.

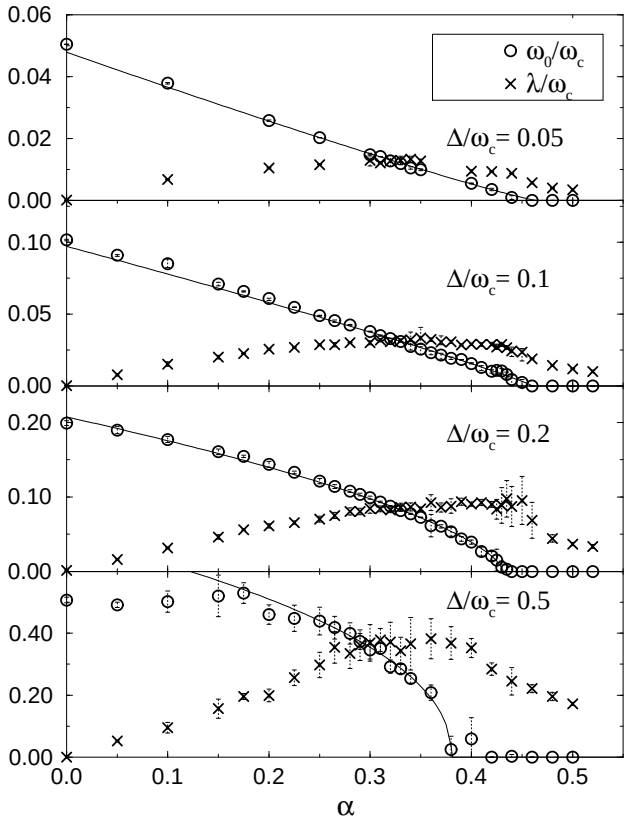

FIG. 7. Tunneling frequency ω_0 (circles) and damping coefficient λ (X's) as functions of the coupling strength α, for $\Delta/\omega_c = 0.05, 0.1, 0.2$ and 0.5, respectively. ω_0 is strictly zero where no error bars are shown. The solid lines are power-law fits.

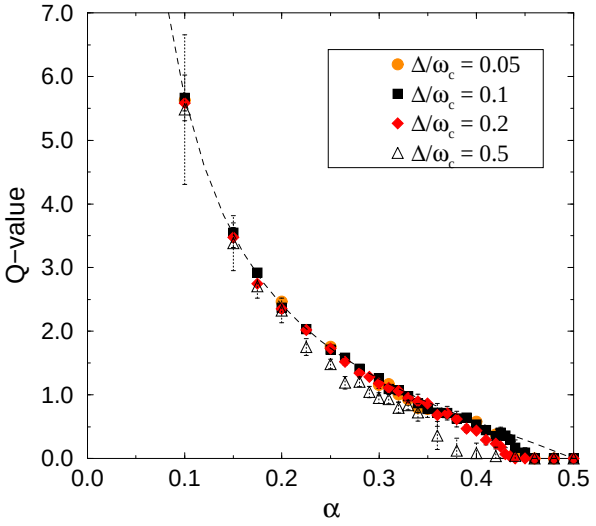

FIG. 8. The Q value $Q = \omega_0/\lambda$ as a function of α, for $\Delta/\omega_c = 0.05, 0.1, 0.2$ and 0.5, respectively. For $\Delta/\omega_c \leq 0.2$ and α not too close to α_c, the data points fall onto a universal scaling curve. The dashed line is expression (34).

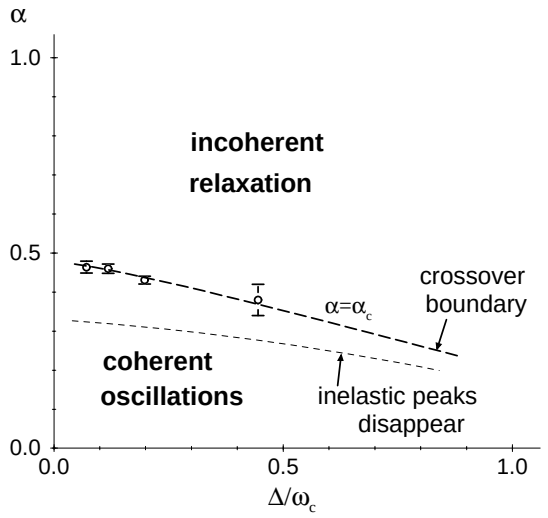

FIG. 9. The phase diagram of the two-state system in the (Δ, α) plane. The four data points for α_c were obtained from power-law fits to $\omega_0(\alpha)$; the dashed line is a guide to the eye only. The values for Δ/ω_c include the cutoff corrections estimated in sec. VIII.

The physical meaning of $\alpha = 1/3$ is simply that the damping coefficient starts to exceed the oscillation frequency.

Within the quasiparticle point of view the transition to strongly damped behavior takes place when the poles coincide with the imaginary axis ($\omega_0 = 0$). For small Δ/ω_c, the equivalence between the two-state system with $\alpha = 1/2$ and the Toulouse limit of the Kondo model provides good reasons to assume that this transition occurs at $\alpha_c = 1/2$. Calculations of the correlation function $P(t)$, which is the conditional average $\langle \sigma_z(t) \rangle$ with the constraint $\sigma_z(t) = 1$ for $t < 0$, support this conclusion.[4] An exact expression[20] for the Q value associated with $P(t)$ is known in the limit $\Delta/\omega_c \to 0$:

$$Q = \cot\left(\frac{\pi}{2}\frac{\alpha}{1-\alpha}\right). \tag{34}$$

This expression matches the data in Fig. 8 almost exactly, for α not too close to 1/2. This is an indication that $P(t)$ and $C(t)$ possess an equivalent structure at intermediate times. The discrepancy near $\alpha = 1/2$ may either indicate a breakdown of the quasiparticle picture, or may arise from the fact that we consider finite values of Δ/ω_c.

Our results indicate a crossover value α_c that is slightly smaller than 1/2. We have to be aware that it is in general a difficult task to extract critical coefficients and critical parameter values from Monte Carlo simulation data. Simulation errors increase significantly near the transition point, and in our case the errors get magnified by the procedure of analytical continuation to the real axis. Nevertheless, according to our results, ω_0 is strictly zero at least for $\alpha \gtrsim 0.48$. However, for $\Delta/\omega_c < 0.1$ the Ising correlation function falls off so fast that the Padé approximation becomes increasingly unreliable. The calculations for $\Delta/\omega_c = 0.05$ and α near its critical value were performed on a lattice of $N = 512$ Ising spins, but simulations with an even larger number would be necessary to confirm the accuracy of the results. These are very difficult to conduct due to the N^2 behavior of the computation time. As we shall see in sec. VIII, cutoff corrections become significant for small Δ/ω_c, and prevent us from approaching the limit $\Delta/\omega_c \to 0$. With cutoff corrections and error bars taken into account, the results presented here allow the conclusion that $\alpha_c = 1/2$ is the correct crossover value[21] in the limit $\Delta/\omega_c \to 0$.

The results of the power-law fits are summarized in the following table (ν is the "critical exponent" of ω_0). The phase diagram of the system is sketched in Fig. 9.

Δ/ω_c	α_c	ν
0.05	0.464 ± 0.015	1.11 ± 0.11
0.1	0.460 ± 0.012	0.91 ± 0.12
0.2	0.431 ± 0.010	0.63 ± 0.09
0.5	0.38 ± 0.04	0.47 ± 0.31

VII. THE BIASED TWO-STATE SYSTEM

We will now investigate the influence of a bias ($\epsilon > 0$) on the dynamical behavior of the system, i.e. one of the states is energetically favored. The spin-spin correlation function, as defined above, then acquires a delta function peak at zero frequency, due to the non-vanishing expectation value $\langle \sigma_z(\tau) \rangle$. If we instead consider the irreducible correlation function $\langle \sigma_z(\tau)\sigma_z(0) \rangle - \langle \sigma_z \rangle^2$, we discover that its Fourier transform is again surprisingly well described by a four-pole structure. The bias shifts the location of the quasiparticle poles in the complex plane, but does not otherwise change the analytic structure of the dominant part. Fig. 10 shows the oscillation frequency ω_0 and damping coefficient λ as a function of ϵ/ω_c, for $\Delta/\omega_c = 0.1$ and three different values of α.

In the first graph, $\alpha = 0.2$, the damping coefficient λ remains largely unaffected by the bias. As we might expect from the undamped case ($\alpha = 0$), where $\omega_0 = \sqrt{\Delta^2 + \epsilon^2}$, the tunneling frequency increases linearly with the bias, in the limit of large ϵ. This leads to an overall linear increase in the Q value. These features were already observed in Sec. IV. The graphs for $\alpha = 0.5$ and $\alpha = 0.75$ show the same qualitative behavior for large ϵ/ω_c. We see that a bias can induce a transition from strongly damped ($\omega_0 = 0$) to oscillatory ($\omega_0 > 0$) behavior. Since the system dwells in the lower-energy state for most of the time, the interaction with the environment is reduced, and damping is less effective in the presence of a bias. At zero temperature and for moderate coupling to the environment ($0.5 \leq \alpha \leq 1.0$), the system will always display oscillatory behavior if the bias exceeds a critical value ϵ_c ($\epsilon_c/\omega_c \simeq 0.01$ for $\Delta/\omega_c = 0.1$, $\alpha = 0.5$, and

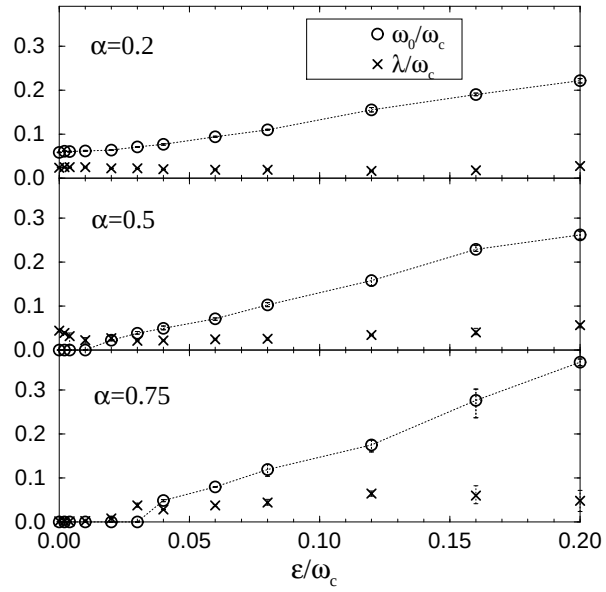

FIG. 10. Tunneling frequency and damping coefficient as a function of the bias ϵ for $\Delta/\omega_c = 0.1$ and different values of α. The biased system favors coherent relaxation.

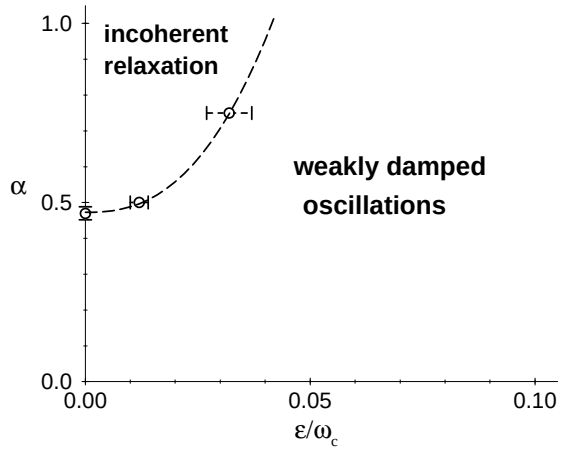

FIG. 11. The phase diagram in the (ϵ, α) plane, for $\Delta/\omega_c = 0.1$

$\epsilon_c/\omega_c \simeq 0.03$ for $\Delta/\omega_c = 0.1$, $\alpha = 0.75$). The resulting phase diagram is sketched in Fig. 11.

At long time scales, the dynamics are governed by the zero-frequency behavior of the spectral function. Fig. 12 shows $\lim_{\omega\to 0} S(\omega)$ as a function of the bias. The theoretical prediction[22] for large ϵ/ω_c is

$$\lim_{\omega\to 0} S(\omega) \sim \left(\frac{\epsilon}{\omega_c}\right)^{4\alpha-6}. \tag{35}$$

This is in good agreement with the results shown.

VIII. SHIBA'S RELATION AND THE TOULOUSE LIMIT

Shiba's relation was originally proven for the Anderson model, but later generalized to the two-state system without[23] and with[22] a bias. It connects the zero-frequency behavior of the spectral function to the static susceptibility as:

$$\lim_{\omega\to 0} S(\omega) = \frac{\pi}{2}\alpha\chi_0^2, \tag{36}$$

where the static susceptibility

$$\begin{aligned}\omega_c\chi_0 &= \lim_{\omega\to 0}\omega_c\chi'(\omega) \\ &= \sum_\tau \Big[\langle\sigma_z(\tau)\sigma_z(0)\rangle - \langle\sigma_z\rangle^2\Big]\end{aligned} \tag{37}$$

can be directly extracted from the Monte Carlo simulations on the Ising system. Shiba's relation therefore constitutes another important check of our numerical approach.

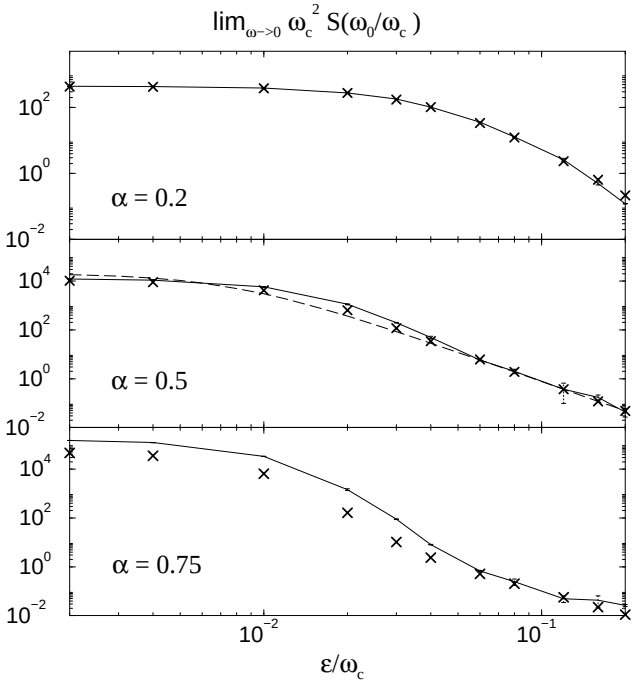

FIG. 12. Zero-frequency limit of $S(\omega)$ as a function of the bias. The solid lines (with error bars) are our simulation results. The 'X' show $S(\omega \to 0)$ as given by Shiba's relation. The dashed line in the graph for $\alpha = 0.5$ is the exact analytical expression (42) for the Toulouse case.

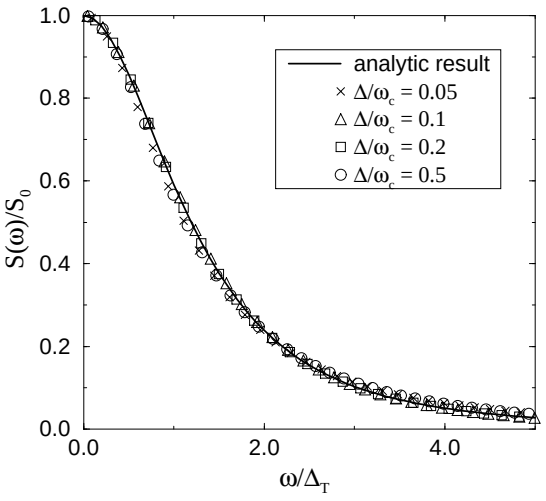

FIG. 13. The spectral function in the Toulouse limit $\alpha = 1/2$. The solid line shows the analytic expression, while the symbols represent numerical results for different values of Δ/ω_c.

In the Toulouse case, $\alpha = 1/2$, the explicit form of the spectral function is given as[4] (note the different normalization of the spins)

$$S(\omega) = \frac{8}{\pi\Delta_T^2}\frac{1}{\left(\frac{\omega}{\Delta_T}\right)^2 + 4}\left[\frac{\Delta_T}{\omega}\tan^{-1}\left(\frac{\omega}{\Delta_T}\right) + \left(\frac{\Delta_T}{\omega}\right)^2 \ln\left(1+\left(\frac{\omega}{\Delta_T}\right)^2\right)\right], \tag{38}$$

where

$$\Delta_T = \frac{\pi}{4}\frac{\Delta^2}{\omega_c}. \tag{39}$$

Figure 13 compares the analytic expression to our numerical results. The simulation data for $0.1 \leq \Delta/\omega_c \leq 0.2$ reproduce the analytical result exactly. Outside this range, the agreement is still good but no longer exact.

At zero frequency, expression (38) reduces to

$$\lim_{\omega\to 0} S(\omega) = \frac{4}{\pi\Delta_T^2}. \tag{40}$$

Equations (36) and (40) allow us to estimate the cutoff corrections to Δ/ω_c (see section II) through the relation

$$\frac{\Delta}{\omega_c} = \frac{4}{\pi}\left(\omega_c\chi_0\right)^{-1/2}. \tag{41}$$

The following table compares the static susceptibility, as given by (37) and calculated from Shiba's relation, and lists the corrected values of Δ/ω_c. Shiba's relation is satisfied to great accuracy for larger values of Δ/ω_c, but the agreement becomes worse for smaller values ($\Delta/\omega_c \lesssim 0.1$). The discrepancy in Δ/ω_c is typically around 10%, but becomes larger for very small Δ/ω_c.

Δ/ω_c	$\omega_c\chi_0$ Ising	$\omega_c^2 S(0)$	$\omega_c\chi_0$ Shiba	err. Shiba	$(\Delta/\omega_c)_{\rm corr}$	err. cutoff
0.05	324	1.19×10^5	389	20%	0.071	41%
0.1	117	1.22×10^4	124.6	6.5%	0.118	18%
0.2	41.4	1.35×10^3	41.5	0.25%	0.198	1.0%
0.5	8.19	53.6	8.26	0.87%	0.445	11.0%

For the biased system, a generalization of expression (40) is given by Lesage and Saleur[22]:

$$\lim_{\omega\to 0} S(\omega) = \frac{4}{\pi}\frac{\Delta_T^2}{\left(\epsilon^2+\Delta_T^2\right)^2}. \tag{42}$$

Figure 12 compares this to the numerical results. The agreement with Shiba's relation is excellent for small α, but only qualitatively right for larger values of $\alpha \gtrsim 1/2$.

IX. CONCLUSIONS

We investigated the dynamical behavior of a two-state system, coupled to a bosonic environment with linear spectral density, in the parameter range $0.05 \leq \Delta/\omega_c \leq 0.5$, $\alpha \leq 0.75$ and $0 \leq \epsilon/\omega_c \leq 0.2$. We found that the crossover from oscillatory behavior to incoherent exponential decay occurs in the vicinity of $\alpha = 1/2$, which corresponds to the Toulouse limit of the anisotropic Kondo model. However, technical difficulties prevent us from obtaining precise answers in the limit of very small Δ/ω_c: The strong nearest-neighbor interaction in the Ising picture causes the imaginary-time correlation function $\mathcal{C}(\omega)$ to fall off very fast, so that we are effectively left with just a small number of data points on which we can base the Padé approximation. Simulations on a larger Ising-spin system would be necessary to yield stable results.

The results presented within the quasiparticle approximation support the conclusion that $\alpha_c = 1/2$ is the correct crossover value in the limit $\Delta/\omega_c \to 0$, but show that $\alpha_c < 1/2$ for finite Δ/ω_c.

For $\alpha > 1/3$, the spectral function $S(\omega)$ does not show any peaks on the real axis at finite frequencies, but is centered around $\omega = 0$. We have seen that the system nevertheless exhibits oscillatory behavior beyond that point, so that $\alpha = 1/3$ does not correspond to a crossover value.

A bias increases the oscillation frequency, in the same way as it does for the decoupled system, and favors coherent oscillations to the extent that a strong enough bias can induce a transition from overdamped relaxation to weakly damped oscillatory behavior. This is true even for rather strong coupling $1/2 < \alpha < 1$.

ACKNOWLEDGMENTS

I wish to thank Sudip Chakravarty for providing me with many of the ideas that made this paper possible, and for continuous intellectual support. This work was supported by a grant from the National Science Foundation, Grant No. DMR 9531575

[1] B. Golding, N. M. Zimmerman, and S. N. Coppersmith, Phys. Rev. Lett. **68**, 998 (1992); K. Chun and N. O. Birge, Phys. Rev. B **54**, 4629 (1996).

[2] S. Chakravarty and P. W. Anderson, Phys. Rev. Lett. **72**, 3859 (1994).

[3] F. Lesage, H. Saleur and S. Skorik, Phys. Rev. Lett. **76**, 3388 (1996) or cond-mat/9512087; see also Ref. 22.

[4] A. J. Leggett, S. Chakravarty, A. T. Dorsey, M. P. A. Fisher, A. Garg, and W. Zwerger, Rev. Mod. Phys. **59**, 1 (1987).

[5] for a recent textbook on the subject, see U. Weiss, *Quantum Dissipative Systems*, World Scientific, Singapore 1993.

[6] L. D. Chang and S. Chakravarty, Phys. Rev. B **31** 154 (1985).

[7] P. W. Anderson and G. Yuval, J. Phys. C **4** 607 (1971).

[8] S. Chakravarty and J. Rudnick, Phys. Rev. Lett. **75**, 501 (1995).

[9] F. Guinea, Phys. Rev. B **32**, 4486 (1985); T. A. Costi, Phys. Rev. Lett. **80**, 1038 (1998) or cond-mat/9712040.

[10] S. Chakravarty, Phys. Rev. Lett. **49**, 681 (1982).

[11] Monte Carlo simulations on the Coulomb Gas Model were first utilized by K. D. Schotte and U. Schotte, Phys. Rev. B **4**, 2228 (1971), to obtain thermodynamic properties of the Kondo model. In contrast to the present approach, these were carried out in the grand canonical ensemble.

[12] P. W. Anderson, G. Yuval and D. R. Hamann, Phys. Rev. B **1**, 4464 (1970).

[13] J. Cardy, J. Phys. A **14**, 1407 (1981).

[14] R. H. Swendsen and J.-S. Wang, Phys. Rev. Lett. **58**, 86 (1987).

[15] H. J. Vidberg and J. W. Serene, J. Low Temp. Phys. **29**, 179 (1977).

[16] note that our definition of the correlation function differs from the widely used definition $C(t) = \mathrm{Re}\,\langle\sigma_z(t)\sigma_z(0)\rangle = \frac{1}{2}\left\langle[\sigma_z(t),\sigma_z(0)]_+\right\rangle$. See the discussion at the end of Sec. V.

[17] see, for example, A. A. Abrikosov, L. P. Gorkov and I. E. Dzyaloshinski, *Methods of Quantum Field Theory in Statistical Physics*, Dover, N.Y. 1975.

[18] A. Fetter and J. Walecka, *Quantum Theory of Many-Particle Systems*, McGraw-Hill 1971, Chapter 3.

[19] T. A. Costi and C. Kieffer, Phys. Rev. Lett. **76**, 1683 (1996) or cond-mat/9601107.

[20] S. Chakravarty and A. J. Leggett, Phys. Rev. Lett. **52**, 5 (1984); F. Lesage and H. Saleur, cond-mat/9712019 and hep-th/9801089.

[21] Recently, J. Stockburger and C. H. Mak, Phys. Rev. Lett. **80**, 2657 (1998) or cond-mat/9802054, arrived at the same conclusion by means of quantum dynamical simulations.

[22] F. Lesage and H. Saleur, Nucl. Phys. B **490**, 543 (1997) or cond-mat/9611025.

[23] M. Sassetti and U. Weiss, Phys. Rev. Lett. **65**, 2262 (1990).